ACS APPLIED MATERIALS & INTERFACES

Research Article

www.acsami.org

Effect of Substrate Morphology Slope Distributions on Light Scattering, nc-Si:H Film Growth, and Solar Cell Performance

Do Yun Kim,*[,†] Rudi Santbergen,[†] Klaus Jäger,[†] Martin Sever,[‡] Janez Krč,[‡] Marko Topič,[‡] Simon Hänni,[§] Chao Zhang,[∥] Anna Heidt,[∥] Matthias Meier,[∥] René A. C. M. M. van Swaaij,[†] and Miro Zeman[†]

[†]Photovoltaic Materials and Devices, Department of Electrical Sustainable Energy, Delft University of Technology, 2600 GA Delft, The Netherlands

[‡]Faculty of Electrical Engineering, University of Ljubljana, Tržaška cesta 25, 1000 Ljubljana, Slovenia

[§]Photovoltaics and Thin-Film Electronics Laboratory, Institute of Microengineering (IMT), École Polytechnique Fédérale de Lausanne (EPFL), 2000 Neuchâtel, Switzerland

[∥]Institute of Photovoltaics, Forschungszentrum Jülich GmbH, Jülich 52425, Germany

ABSTRACT: Thin-film silicon solar cells are often deposited on textured ZnO substrates. The solar-cell performance is strongly correlated to the substrate morphology, as this morphology determines light scattering, defective-region formation, and crystalline growth of hydrogenated nanocrystalline silicon (nc-Si:H). Our objective is to gain deeper insight in these correlations using the slope distribution, rms roughness (σ_{rms}) and correlation length (l_c) of textured substrates. A wide range of surface morphologies was obtained by Ar plasma treatment and wet etching of textured and flat-as-deposited ZnO substrates. The σ_{rms}, l_c and slope distribution were deduced from AFM scans. Especially, the slope distribution of substrates was represented in an efficient way that light scattering and film growth direction can be more directly estimated at the same time. We observed that besides a high σ_{rms}, a high slope angle is beneficial to obtain high haze and scattering of light at larger angles, resulting in higher short-circuit current density of nc-Si:H solar cells. However, a high slope angle can also promote the creation of defective regions in nc-Si:H films grown on the substrate. It is also found that the crystalline fraction of nc-Si:H solar cells has a stronger correlation with the slope distributions than with σ_{rms} of substrates. In this study, we successfully correlate all these observations with the solar-cell performance by using the slope distribution of substrates.

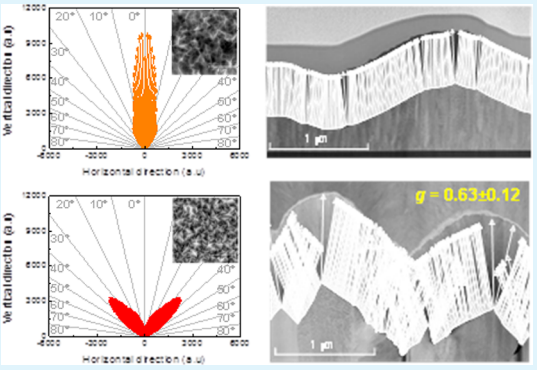

KEYWORDS: *surface morphology, light scattering, film growth, nc-Si:H, defective layer, solar cell*

1. INTRODUCTION

Light management is a key technique for obtaining high-efficiency thin-film silicon solar cells.[1,2] For this purpose light scattering needs to be optimized. This light scattering is strongly dependent on the substrate morphology.[3] Experiments and simulations have shown that rough interfaces increase the light scattering, resulting in better light absorption compared to flat substrates.[4,5] However, in the literature, it has been reported that defective regions are formed in hydrogenated nanocrystalline silicon (nc-Si:H), especially when the film is grown on a very rough substrate.[6,7] Nasuno et al. observed that for nc-Si:H grown on rough substrates columnar growth is limited by collision of columns and that many grain boundaries are present.[8] Python et al. showed that defective regions were present in the valleys of the steep surfaces and could estimate the density of cracks by taking into account the valley curvature radii.[9] The presence of these defective regions in nc-Si:H is known to decrease the open-circuit voltage (V_{oc}) of nc-Si:H solar cells and subsequently decreases device performance.[8−11]

It is well-known that the crystalline silicon growth can be controlled by varying the hydrogen dilution during silicon film growth.[12−14] On the other hand, it is also reported that the chemical and crystallographic nature, and the morphology of substrates largely influences the crystalline growth resulting in a different crystalline fraction (X_c) of nc-Si:H.[15,16] X_c affects the mobility gap (E_μ) of intrinsic nc-Si:H, which in turn influences the V_{oc} of nc-Si:H solar cells.[16] nc-Si:H consists of amorphous and crystalline mixed phases and each phase has a different absorption coefficient. Therefore, when nc-Si:H films have different X_c, they will absorb sunlight quite differently and, as a result, J_{sc} as well as V_{oc} can be different. To summarize, the substrate morphology is linked to three particularly important factors, which strongly influence the solar-cell performance: (1) light scattering (J_{sc}); (2) defective regions (V_{oc} and FF); and (3) crystalline fraction (V_{oc} and J_{sc}).

Received: August 12, 2014
Accepted: November 24, 2014
Published: November 24, 2014

   dx.doi.org/10.1021/am5054114 | *ACS Appl. Mater. Interfaces* 2014, 6, 22061−22068

The substrate morphology is generally characterized by the root-mean-square (rms) roughness (σ_{rms}), which is a measure for vertical feature size.[17−20] This σ_{rms}, however, describes only the height distribution of substrates; their unique characteristics, such as a slope of surfaces, are not taken into account. This slope represents the degree of steepness and, consequently, a slope distribution of substrates over entire area can be considered as their fingerprints. Nevertheless, the slope distribution of substrates has been hardly used to describe their morphology.[21,22] Numerous studies have shown partial correlations of substrate morphology with (a) light scattering, (b) defective region formation, or (c) crystalline growth. However, an investigation covering all these aspects at the same time has not been carried out yet.

In this contribution, we provide a deeper overview of how the substrate morphology, especially the slope distributions of the substrates besides σ_{rms} and correlation length (l_c),[23] affects light scattering, defective-region formation, crystalline growth, and thereby nc-Si:H solar cell performance. First of all, we characterize substrate morphologies using various parameters such as σ_{rms}, l_c, and surface slope distributions of substrates. In particular, we show surface slope distributions in an efficient way, from which film growth directions and light scattering can be estimated more directly. Subsequently, we correlate these substrate morphologies to light scattering, crystalline growth and defective region formation. Finally, we show that the external parameters of nc-Si:H solar cells can all be understood in terms of the above-mentioned observations.

2. SURFACE MORPHOLOGY OF ZNO SUBSTRATES

In this work, various transparent conductive oxide (TCO) substrates were investigated and characterized. These samples were fabricated by Delft University of Technology (TU Delft, The Netherlands) and École Polytechnique Fédérale de Lausanne (EPFL, Switzerland), respectively. ZnO:B from EPFL was fabricated by low-pressure chemical vapor deposition (LPCVD)[24] and the ZnO:Al from TU Delft was fabricated by radio frequency (RF, 13.56 MHz) sputtering using a 2% Al-doped ZnO target. The sheet resistance (R_S) of these as-deposited ZnO:B and ZnO:Al are 8.0 and 6.0 Ω/□ at nominal thickness of 5.0 and 1.3 μm, respectively. Atomic force microscopy (AFM) scans of 256 × 256 points over an area of 10 × 10 μm^2 on the ZnO substrates were taken to determine the substrate morphologies, which in turn were used for deducing the σ_{rms} and l_c. The fundamental information on all ZnO substrates used in this study is summarized in Table 1. The as-deposited ZnO by EPFL (A-0) is known to be very rough. In this case the roughness is reduced by surface treatment under Ar plasma. In A-5 to A-45, the treatment time was varied from 5 to 45 min, which reduces σ_{rms} while increasing l_c. The thickness of ZnOs is almost unchanged after the treatment; the nominal thickness of A-0 to A-45 is 5.0 μm. The as-deposited ZnO by TU Delft (B-0) is flat and the roughness was increased by wet etching in 0.5% HCl. In B-20 to B-80 the etching time was varied from 20 to 80 s. The results shown in Table 1 confirm that wet etching of the sputtered ZnO increases both σ_{rms} and l_c. Note that the R_S of B-80 (10.3 Ω/□) is slightly higher than that of B-0 (6.0 Ω/□) because its thickness is reduced from 1.3 to 0.7 μm after 80 s of wet-etching.

Table 1. Fundamental Information of ZnO Substrates Used in This Study

ID	institute	deposition system	σ_{rms} (nm)	l_c (nm)	texturing conditions
A-0	EPFL	LPCVD	158	315	as-deposited
A-5	EPFL	LPCVD	156	358	5 min Ar plasma
A-20	EPFL	LPCVD	145	377	20 min Ar plasma
A-45	EPFL	LPCVD	113	500	45 min Ar plasma
B-0	TU Delft	RF sputtering	<5		as-deposited
B-20	TU Delft	RF sputtering	122	370	20 s wet etching
B-40	TU Delft	RF sputtering	137	683	40 s wet etching
B-60	TU Delft	RF sputtering	162	860	60 s wet etching
B-80	TU Delft	RF sputtering	200	1270	80 s wet etching

From this height data obtained from AFM, a surface consisting of triangular facets was created that accurately represents the scanned surface morphology. Subsequently, we determined the surface normal vector (SNV) distributions from all facets in the AFM scan. The slope of a facet is defined as the angle between the surface normal and the *z*-direction (height direction). In Figure 1a−d, slope distributions of A-0, A-45, B-20, and B-80 are shown with AFM images (the inset of the figure), respectively. The absolute value of the surface normal vectors represents the number of vectors having the same angles. Note that in the figures of this paper, we consistently use different colors for specific samples.

From the AFM image of the inset in Figure 1a, it can be seen that the surface morphology of A-0 is sharp and steep, and that it has a pyramidal shape. In this case the overall slope distribution of this ZnO surface mainly ranges from 20 to 50° with an average slope angle (θ_{av}) of 30.6°, which is fairly steep. After the Ar plasma treatment (*A-45*) the surface is smoothened as can be seen from the inset of Figure 1b. For A-45, dominant slopes are distributed at 0 to 10° and the density of steep slopes has been significantly reduced, meaning that the surface becomes smoother. This A-45 substrate does not have a clear pyramidal shape anymore but rather an intermediate shape between pyramidal and craterlike. Nevertheless, it should be noted that A-45 still has a considerable fraction of slopes higher than 20°, resulting in θ_{av} of 11.4°.

On the other hand, for B-series ZnOs (B-0 to B-80), we observed two phases during wet etching. First, the flat regions (slope 0°) are reduced and with increasing etching times relatively shallow slopes appear as the flat-as-deposited ZnO is roughened. In Figure 1c, it can be seen that for sample B-20 (i) a slope of 0° is relatively uncommon, (ii) dominant slopes are distributed at angles below 10°, and (iii) no slopes above 20° are observed. This result reveals that after 20 s of etching relatively smooth regions with a small crater size are prevalent.

When increasing the etching time further, the flat region (slope 0°) again increases and slopes between 10° and 20° become dominant as larger crater-like surfaces are formed. We found that after 80-s etching (*B-80*) the slopes below 10° are considerably reduced, as shown in Figure 1(d). This substrate has the highest σ_{rms}, but overall slopes are relatively shallow.

3. LIGHT SCATTERING PROPERTIES

In order to investigate the optical properties of these samples, we measured haze in transmission (H_T) for the A-0, A-45, B-20, and B-80 samples as shown in Figure 2a. It is observed that the H_T of A-0 is much higher than that of A-45 over the entire wavelength range. This significantly higher H_T for A-0 is due to its rougher surface morphology. This result is accompanied by preferential light scattering into very large angles, as can be seen

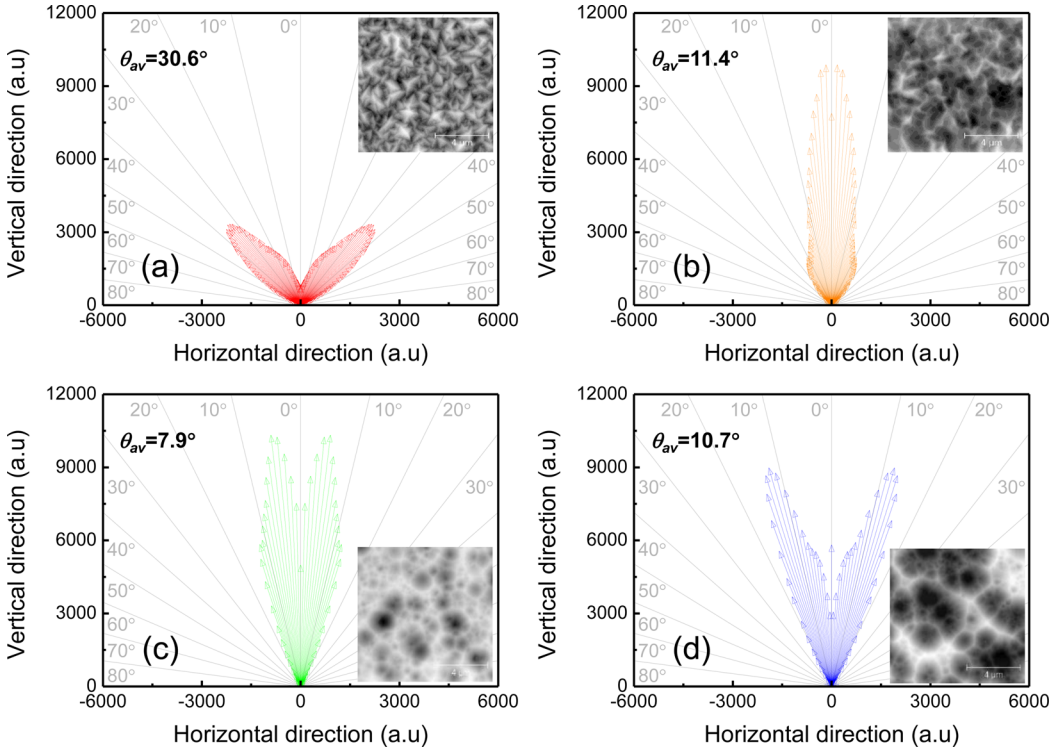

Figure 1. Surface normal vector (SNV) distribution (or slope distribution) and AFM images of (a) A-0, (b) A-45, (c) B-20, and (d) B-80 ZnO substrates. The gray line is a guide for the eyes showing the angle of SNVs to vertical direction.

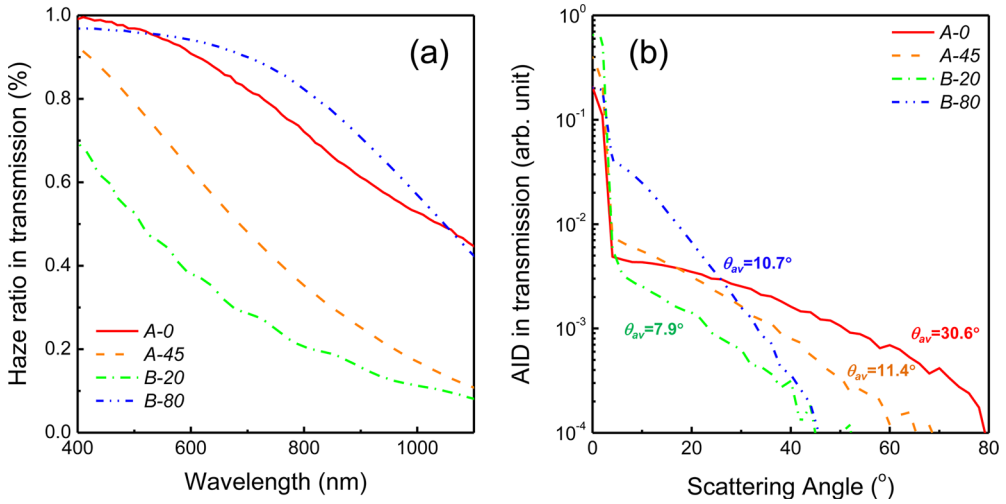

Figure 2. (a) Haze in transmission (H_T) and (b) angular intensity distribution in transmission (AID_T) of A-0, A-45, B-0, and B-45 ZnO substrates measured in air. For the AID_T measurement, a light wavelength of 850 nm was used.

from the angular intensity distribution in transmission (AID_T) of these ZnO substrates shown in Figure 2b.

Similar behavior is observed for B-20 and B-80. The H_T of B-80 is much larger than that of B-20 because B-80 has higher σ_{rms}. Interestingly, we observe that the increase in H_T for B-80 arises from light scattering into relatively small angles, which is quite different from the results observed for A-0. It is clear that the AID_T shown in Figure 2b has a strong correlation with slope distributions shown in Figure 1a–d. As the slope distribution becomes dominant at higher angles, resulting in higher θ_{av}, the transmitted light is also found to be more pronounced at larger scattering angles (see red and orange lines in Figure 2b). On the other hand, when the average slope of the surfaces becomes small and the density of flat regions increases, resulting in lower θ_{av}, the light is preferentially scattered into smaller scattering angles (see blue and green lines). Jäger et al. observed similar trends from optical simulations carried out using the scalar scattering theory.[23] These simulations showed that the lateral feature size, which is proportional to l_c, strongly influences the photocurrent of thin-film silicon solar cells when σ_{rms} is kept constant (i.e., effectively changing the average slope for randomly textured morphologies, which corresponds to the ratio between σ_{rms} and l_c). Our experimental results are in good agreement with the simulation trends.

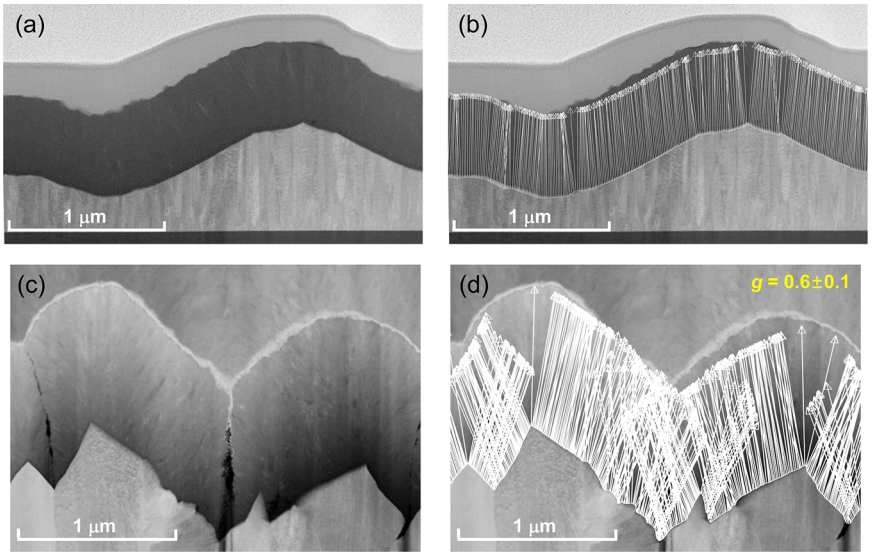

Figure 3. TEM cross sections of p-i-n nc-Si:H solar cells grown on C-80 (a) without fitted growth vectors and (b) with fitted growth vectors; and grown on D-0 (c) without fitted growth vectors and (d) with fitted growth vectors.

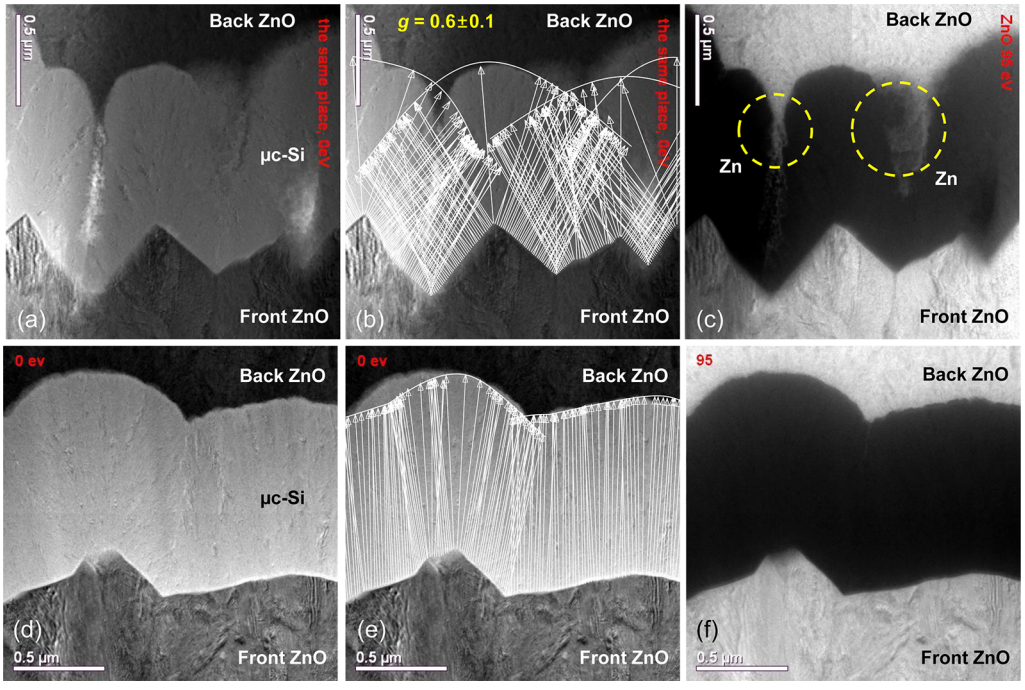

Figure 4. TEM images of D-0 (a) without fitted growth vectors, (b) with fitted growth vectors, and (c) EF-TEM image of D-0. TEM images of D-45 (d) without fitted growth vectors, (e) with fitted growth vectors, and (f) EF-TEM image of D-45..

4. NC-SI:H FILM GROWTH AND DEFECTIVE REGION FORMATION

In order to study the growth of nc-Si:H on different substrate morphologies, we measured transmission electron microscopy (TEM) cross-section of solar cells and used the growth model developed by Sever et al. that considers both conformal and isotropic growth.[25] In this model, the *g*-value, which is an indication of the degree of the isotropic growth, is a fit parameter. The isotropic growth vector which is perpendicular to the surface[25] is identical to the SNV discussed above. Therefore, the slope distributions shown in Figure 1a–d can also be interpreted as the isotropic growth vector distributions of substrates. Hence, this can be an approximate measure of how deposited films will grow.

For this study, the solar cells were fabricated by TU Delft, hereafter named C-0 to C-80 (on B-0 to B-80 substrates), and EPFL, hereafter referred to as D-0 to D-45 (on A-0 to A-45 substrates), depending on the used substrates. The solar cells fabricated by EPFL have the following structure: front ZnO/p-nc-SiO_x:H/i-nc-Si:H/n-nc-SiO_x:H/back ZnO/Ag contact,[26] whereas solar cells by TU Delft have a similar structure, but no back ZnO deposited.

We measured energy-filtered transmission electron microscopy (EF-TEM) to obtain element distributions, especially Zn, in solar-cell cross sections. The TEM and EF-TEM of solar cells were measured at Forschungszentrum Jülich (FZJ).

dx.doi.org/10.1021/am5054114 | *ACS Appl. Mater. Interfaces* 2014, 6, 22061–22068

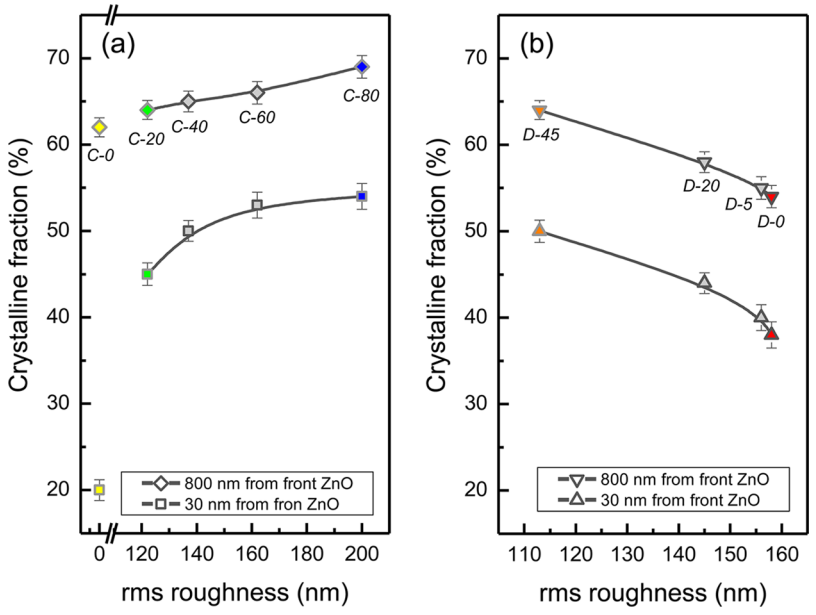

Figure 5. Crystalline fraction of nc-Si:H solar cells for (a) C-0, C-20, C-40, C-60, C-80, (b) D-0, D-5, D-20, and D-45 as a function of rms roughness of substrates.

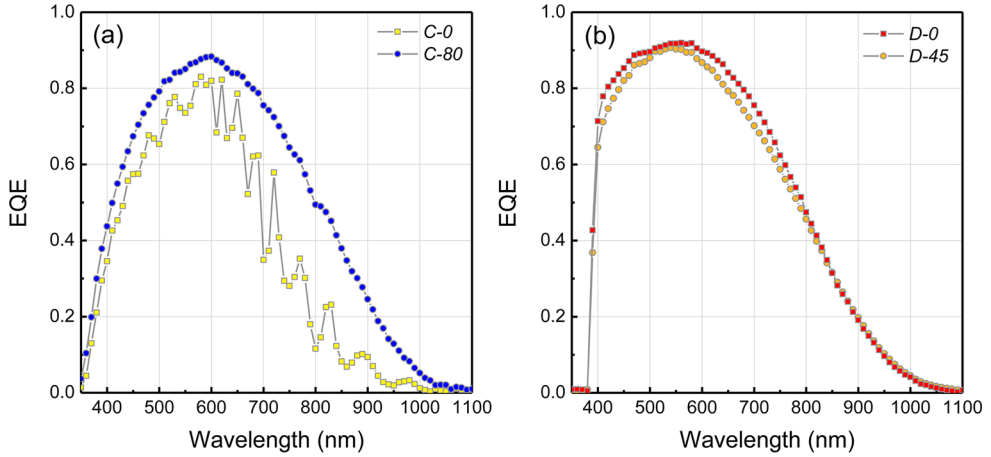

Figure 6. External quantum efficiency (EQE) of (a) C-0 and C-80, and (b) D-0 and D-45.

In Figure 3a we show the original TEM cross-section of C-80. In Figure 3b, the fitted growth vectors are included on this TEM image. In this case the slopes of C-80 are relatively shallow and therefore the isotropic growth vector is very similar to the conformal growth vector. As a result the simulated growth is not very sensitive to the *g*-value. In any case, Figure 3b shows that the fitted growth vectors hardly overlap each other. On the other hand, for D-0 a *g*-value of 0.6 is used to obtain the best fit and it is clearly observed that the fitted growth vectors largely overlap, as shown in Figure 3d. In this case, huge defective regions are present exactly at the same locations where the growth vectors overlap, as can be seen in Figure 3c. The most likely reason for this is that nc-Si:H columns collide more easily with each other during the columnar growth, leading to the formation of defective regions. Therefore, it is clear that these defective regions are directly related to the overlap of growth vectors and, therefore, substrate morphologies. This result is in good agreement with earlier observations.[8−10,25,27] Considering the σ_{rms} of A-0 (158 nm) and B-80 (200 nm), the formation of defective regions is apparently not so much dependent on σ_{rms}, but more on the slope distributions of the substrates.

In Figure 4a, b, we again show TEM images of D-0 with and without fitted growth vectors, respectively. However, this time, an EF-TEM image of the same part of the sample is also presented in Figure 4c.

In EF-TEM, only electrons with particular kinetic energies contribute to the output image. Therefore, the chemical composition of the sample can be studied by EF-TEM. In Figure 4c, bright regions represent a layer containing Zn atoms, which are assumed to originate from the back ZnO:B when deposited on top of the nc-Si:H layer as indicated by the yellow circles. As mentioned above, there are specific locations where fitted growth vectors overlap substantially and defective regions are formed, which are known to be porous.[28] The EF-TEM image now reveals that Zn is mainly present at those locations, which is similar to results reported elsewhere in the literature, where it is reported that this Zn is mainly present in the form of ZnO.[28] This implies that these defective and porous regions are

prone to favor inclusion of ZnO:B when depositing the back ZnO:B by LPCVD.

In Figure 4d–f, TEM and EF-TEM images of D-45 are shown. In this case, the growth of nc-Si:H deposited on this relatively smooth substrate (A-45) is found to be conformal. The overlap of fitted growth vectors and the formation of defective regions are considerably reduced. In this case, we did not observe the defective regions where ZnO can be incorporated.

5. NC-SI:H CRYSTALLINE FRACTION

To evaluate the crystalline fraction (X_c) of nc-Si:H solar cells on different substrates, we carried out Raman measurements with a 514 nm laser. The X_c is subsequently determined by

$$X_c = \frac{I_{520} + I_{510}}{I_{520} + I_{510} + I_{480}} \quad (1)$$

where I_{520}, I_{510}, and I_{480} indicate the integrated area of fitted Gaussian peaks centered at 520, 510, and 480 cm^{-1}, respectively.[29−31] In order to obtain the X_c at different depths in the nc-Si:H solar cells, we measured Raman spectra of solar cells from the n-layer side by alternating Raman measurements and reactive ion etching (RIE) processes repetitively. For this RIE process, we used a gas mixture of CF_4 (70 sccm), SF_6 (10 sccm), and O_2 (10 sccm) as an etchant source at room temperature. The process pressure and radio frequency (RF) power density were kept constant at 0.05 mbar and 340 mW/cm^2, respectively. In Figures 5a and 6b, X_c of nc-Si:H solar cells fabricated on different substrates are presented, which are measured at a positions of ∼30 and ∼800 nm from the front ZnO. In most cases we observe that X_c is at least 15% larger at a distance of ∼800 nm from front ZnO compared to X_c near the front ZnO (distance ∼30 nm) regardless of the substrate roughness. This means that in all cases the crystalline fraction gradually increases during film deposition, which is well-known phenomena for nc-Si:H growth.[12,32] For the C-series, X_c increases as σ_{rms} increases, whereas for the D-series, X_c decreases as σ_{rms} increases. This implies that X_c cannot be simply correlated to σ_{rms} of the substrates only, but that other factors play a role as well.

There are two possible ways to explain this observation. First, it could be related to the slope distribution. We observe that the density of flat regions (slope 0°) increase for C-series solar cells, whereas they decrease for D-series solar cells as σ_{rms} increased (see Figure 1a–d). This implies that crystalline silicon growth is favorable for surfaces with more flat regions. The nucleation density (n_d) affecting X_c of nc-Si:H is nearly independent of substrate morphologies.[15] We therefore speculate that when flat regions are less frequent, the collision of nc-Si:H columns becomes more frequent. This frequent collision of columns likely suppresses crystalline growth, resulting in lower X_c.

Second, the different crystallographic nature of substrates can influence X_c.[15,33] It should be noted that C-0 (as-deposited) shows the lowest X_c at initial growth stage even though it is deposited on the flattest substrate. Considering the fact that X_c of both C- and D-series solar cells increases with increasing etching time, we think that after either wet etching or Ar plasma treatment different crystallographic planes might be exposed. Consequently, the crystallographic nature of A-0 and B-0 is changed in a way favorable for crystalline silicon growth.

6. SOLAR-CELL PERFORMANCE

In Figure 6, we present the external quantum efficiency (EQE) of nc-Si:H solar cells prepared in this study. We also measured illuminated current density versus voltage ($J-V$) characteristics under standard test conditions (AM 1.5, 1000 W/m^2, and 25 °C) for solar cell samples. All the external solar cell parameters tabulated in Table 2 are the average values of the best 5 solar cells for each substrate. The maximal standard deviation in the measured parameters is 2 mV for the V_{oc}, 0.05 mA/cm^2 for the J_{sc}, 0.01 for the FF, and 0.07% for the efficiency η.

Table 2. Photovoltaic Parameters of nc-Si:H Solar Cells Grown on Different Substrates

ID	substrate	institute	V_{oc} (V)	J_{sc} (mA/cm^2)	FF	efficiency (%)
C-0	B-0	TU Delft	0.536	16.30	0.68	5.96
C-20	B-20	TU Delft	0.544	22.20	0.68	8.21
C-80	B-80	TU Delft	0.544	23.02	0.69	8.64
D-0	A-0	EPFL	0.468	23.64	0.63	6.97
D-45	A-45	EPFL	0.564	22.74	0.71	9.11

For both the solar cells prepared by EPFL and TU Delft, EQEs are enhanced over the entire measured wavelength range and thereby J_{sc} are increased as σ_{rms} increases. We ascribe these enhancements of EQEs mainly to the improved light in-coupling and light scattering by the rougher surface.[34] It is well-known that the EQE can be reduced by absorption in the TCO especially when the light is trapped or when the TCO is thick. Therefore, because of the decreased ZnO thickness after the 80 s wet-etching process (B-80), the parasitic absorption of ZnO is reduced and this may also explain a part of observed increase in EQEs. Although the R_S of B-80 was higher than that of B-0 because of the reduced ZnO thickness as mentioned in Section 2, the FF of C-80 is unaffected because the R_S of B-80 is still sufficiently low. In addition, we did not observe any defective regions for C-80 and therefore the FF is not reduced. One would expect cells with higher X_c to show lower V_{oc}. However, C-0 and C-80 show the opposite trend. Since the V_{oc} is proportional to the logarithm of the photogenerated current and reciprocal to the dark saturation current,[35] the increase in V_{oc} could be attributed to the increase in photogenerated current. On the other hand, even though X_c of D-0 was lower than that of D-45, V_{oc} and FF are lower. It should be noted that there are large defective regions in the nc-Si:H grown on the rough substrate (D-0). This can reduce V_{oc} and FF of solar cells by increasing the density of shunt paths, and thereby the leakage current density[10] and carrier recombination at those defects.[8] Moreover, we observed the presence of Zn in the defective regions of the nc-Si:H absorber layer for D-0, originating from the deposition of the back ZnO:B. We think that the decreased V_{oc} and *FF* of the solar cell can be attributed to the presence of the defective regions and likely also to the ZnO which is contained in these defective regions.[28,36] Therefore, the performance of *D-0* is significantly deteriorated, even though D-0 produces a high photo current density due to better light scattering. To summarize, these solar-cell results can be understood deeply in terms of light scattering, the presence of defective regions, and the crystalline growth.

7. DISCUSSION

We have provided a deeper overview of the ways in which the ZnO substrate morphology affects light scattering, defective

region formation and crystalline growth of nc-Si:H and thereby nc-Si:H solar-cell performance. These correlations now enable us to propose design guidelines for fabricating the most suitable nc-Si:H solar cell substrates. When ZnO substrates have σ_{rms} larger than 15 nm, light scattering begins to be observed.[37] Once light scattering occurs, one also needs to consider the slope distribution of the substrate. Slopes larger than at least 20° are required to scatter a significant fraction of the incident light into oblique directions to promote light trapping. However, the dominant slopes should remain below 20−30° to avoid defective region formation. These slopes of 20−30° correspond to opening angles of 120−140°, which are similar to the critical opening angles found in literature.[38,39] Finally substrates with steeper slopes can give rise to reduced crystalline fractions under identical deposition conditions, resulting in higher V_{oc}. However, with dominant slopes above 20−30°, V_{oc} can drop substantially because of the defective region formation. Using A-45 substrate, which is smooth but still enables sufficient light scattering, Hänni et al. already reported the 10.69% world-record nc-Si:H solar cell with i-layer thickness of 2 μm.[40] In addition, Sai et al. reported a 10.50% nc-Si:H solar cell on a honeycomb-textured substrate with an optimized aspect ratio and i-layer thickness.[41] They observed that defective regions could be formed depending on the aspect ratio and i-layer thickness.[42] From these articles, it is clear that substrate morphology must be carefully studied and controlled (i) to ensure defect-less nc-Si:H growth, (ii) to maintain sufficient light scattering, and ultimately (iii) to obtain a high-performance nc-Si:H solar cell.

8. CONCLUSION

In this study, we investigated the effect of surface morphologies of different ZnO substrates on light scattering, nc-Si:H film growth, defective region formation and thereby solar cell performance. In particular, we characterize the morphology using slope distributions of the substrates, obtained from AFM scans. When a substrate contains dominant slope distributions at very high angles and hardly any flat regions, light is efficiently scattered into very large angles resulting in high J_{sc}. However, modeled growth vectors were also found to be largely overlapping each other and we confirmed that defective regions are present exactly at those locations of overlap (D-0). In this case, we also confirmed by EF-TEM that in those locations Zn atoms were distributed within nc-Si:H and that presumably the ZnO layer at the back contact is the source for this Zn. We also observed that the crystalline fraction of solar cells correlates more strongly to the slope distribution than to σ_{rms}. We speculate that flat surfaces are favorable for crystalline growth in nc-Si:H whereas crystalline growth is suppressed by rough substrates. It is found that the V_{oc} and FF dropped for the nc-Si:H solar cell deposited on the rough substrate, because of the presence of defective regions and Zn in the nc-Si:H layer. In this contribution, we present the correlation between substrate morphologies, light scattering, film growth, crystalline growth, defective region formation. This gives a deeper overview of all the ways in which substrate morphology affects the performance of nc-Si:H solar cells. It allowed us to propose design rules for fabricating suitable substrate morphologies for nc-Si:H solar cells.

AUTHOR INFORMATION

Corresponding Author

*E-mail: d.kim@tudelft.nl.

Notes

The authors declare no competing financial interest.

ACKNOWLEDGMENTS

This work was carried out in the framework of the FP7 project "Fast Track", funded by the EC under grant agreement 283501. The authors thank, Michael Ghosh of the Forschungszentrum Jülich, and Michael Stückelberger, Matthieu Despeisse, Mathieu Boccard, and Jan-Willem Schüttauf of PV-lab (EPFL) for the supply of samples. We thank the Institute of Microstructure Research (PGI5) of the Forschungszentrum Jülich for their TEM support. We thank Guangtao Yang, Martijn Tijssen, Stefaan Heirman, and Remko Koornneef from PVMD group of Delft University of Technology for the valuable discussions.

REFERENCES

(1) Müller, J.; Rech, B.; Springer, J.; Vanecek, M. TCO and Light Trapping in Silicon Thin Film Solar Cells. *Sol. Energy* **2004**, *77*, 917−930.

(2) Poruba, A.; Fejfar, A.; Remeš, Z.; Špringer, J.; Vaněček, M.; Kočka, J.; Meier, J.; Torres, P.; Shah, A. Optical Absorption and Light Scattering in Microcrystalline Silicon Thin Films and Solar Cells. *J. Appl. Phys.* **2000**, *88*, 148−160.

(3) Kluth, O.; Rech, B.; Houben, L.; Wieder, S.; Schöpe, G.; Beneking, C.; Wagner, H.; Löffl, A.; Schock, H. W. Texture Etched ZnO:Al Coated Glass Substrates for Silicon Based Thin Film Solar Cells. *Thin Solid Films* **1999**, *351*, 247−253.

(4) Jäger, K.; Zeman, M. A Scattering Model for Surface-Textured Thin Films. *Appl. Phys. Lett.* **2009**, *95*, 171108−1−171108−3.

(5) Jäger, K.; Fischer, M.; van Swaaij, R. A. C. M. M.; Zeman, M. A Scattering Model for Nano-Textured Interfaces and Its Application in Opto-Electrical Simulations of Thin-Film Silicon Solar Cells. *J. Appl. Phys.* **2012**, *111*, 083108−1−083108−9.

(6) Meier, J.; Dubail, S.; Golay, S.; Kroll, U.; Faÿ, S.; Vallat-Sauvain, E.; Feitknecht, L.; Dubail, J.; Shah, A. Microcrystalline Silicon and the Impact on Micromorph Tandem Solar Cells. *Sol. Energy Mater. Sol. Cells* **2002**, *74*, 457−467.

(7) Bugnon, G.; Parascandolo, G.; Söderström, T.; Cuony, P.; Despeisse, M.; Hanni, S.; Holovsky, J.; Meillaud, F.; Ballif, C. A New View of Microcrystalline Silicon: The Role of Plasma Processing in Achieving a Dense and Stable Absorber Material for Photovoltaic Applications. *Adv. Funct. Mater.* **2012**, *22*, 3665−3671.

(8) Nasuno, Y.; Kondo, M.; Matsuda, A. Effects of Substrate Surface Morphology on Microcrystalline Silicon Solar Cells. *Jpn. J. Appl. Phys.* **2001**, *40*, L303−L305.

(9) Python, M.; Madani, O.; Dominé, D.; Meillaud, F.; Vallat-Sauvain, E.; Ballif, C. Influence of the Substrate Geometrical Parameters on Microcrystalline Silicon Growth for Thin-Film Solar Cells. *Sol. Energy Mater. Sol. Cells* **2009**, *93*, 1714−1720.

(10) Python, M.; Vallat-Sauvain, E.; Bailat, J.; Domine, D.; Fesquet, L.; Shah, A.; Ballif, C. Relation between Substrate Surface Morphology and Microcrystalline Silicon Solar Cell Performance. *J. Non-Cryst. Solids* **2008**, *354*, 2258−2262.

(11) Biron, R.; Hänni, S.; Boccard, M.; Pahud, C.; Söderström, K.; Duchamp, M.; Dunin-Borkowski, R.; Bugnon, G.; Ding, L.; Nicolay, S.; Parascandolo, G.; Meillaud, F.; Despeisse, M.; Haug, F.-J.; Ballif, C. New Progress in the Fabrication of N−I−P Micromorph Solar Cells for Opaque Substrates. *Sol. Energy Mater. Sol. Cells* **2013**, *114*, 147−155.

(12) Wronski, C. R.; Von Roedern, B.; Kołodziej, A. Thin-Film Si:H-Based Solar Cells. *Vacuum* **2008**, *82*, 1145−1150.

(13) Layadi, N.; Roca i Cabarrocas, P.; Drévillon, B.; Solomon, I. Real-Time Spectroscopic Ellipsometry Study of the Growth of Amorphous and Microcrystalline Silicon Thin Films Prepared by Alternating Silicon Deposition and Hydrogen Plasma Treatment. *Phys. Rev. B* **1995**, *52*, 5136−5143.

(14) Koh, J.; Ferlauto, A. S.; Rovira, P. I.; Wronski, C. R.; Collins, R. W. Evolutionary Phase Diagrams for Plasma-Enhanced Chemical Vapor Deposition of Silicon Thin Films from Hydrogen-Diluted Silane. *Appl. Phys. Lett.* **1999**, *75*, 2286−2288.
(15) Vallat-Sauvain, E.; Bailat, J.; Meier, J.; Niquille, X.; Kroll, U.; Shah, A. Influence of the Substrate's Surface Morphology and Chemical Nature on the Nucleation and Growth of Microcrystalline Silicon. *Thin Solid Films* **2005**, *485*, 77−81.
(16) Kim, D. Y.; van Swaaij, R. A. C. M. M.; Zeman, M. Optical and Electrical Simulation of μc-Si:H Solar Cells: Effect of Substrate Morphology and Crystalline Fraction. *IEEE J. Photovoltaics* **2014**, *4*, 22−27.
(17) Lee, J. B.; Kwak, S. H.; Kim, H. J. Effects of Surface Roughness of Substrates on the C-axis Preferred Orientation of ZnO Films Deposited by R.F. Magnetron Sputtering. *Thin Solid Films* **2003**, *423*, 262−266.
(18) Berginski, M.; Hüpkes, J.; Schulte, M.; Schöpe, G.; Stiebig, H.; Rech, B.; Wuttig, M. The Effect of Front ZnO:Al Surface Texture and Optical Transparency on Efficient Light Trapping in Silicon Thin-Film Solar Cells. *J. Appl. Phys.* **2007**, *101*, 074903−1−074903−11.
(19) Faÿ, S.; Feitknecht, L.; Schlüchter, R.; Kroll, U.; Vallat-Sauvain, E.; Shah, A. Rough ZnO Layers by LP-CVD Process and Their Effect in Improving Performances of Amorphous and Microcrystalline Silicon Solar Cells. *Sol. Energy Mater. Sol. Cells* **2006**, *90*, 2960−2967.
(20) Hu, J.; Gordon, R. G. Textured Aluminum-Doped Zinc Oxide Thin Films from Atmospheric Pressure Chemical-Vapor Deposition. *J. Appl. Phys.* **1992**, *71*, 880−890.
(21) Meier, M.; Paetzold, U. W.; Prömpers, M.; Merdzhanova, T.; Carius, R.; Gordijn, A. UV Nanoimprint for the Replication of Etched ZnO:Al Textures Applied in Thin-Film Silicon Solar Cells. *Prog. Photovoltaics* **2013**, DOI: 10.1002/pip.2382.
(22) Zhang, W.; Paetzold, U. W.; Meier, M.; Gordijn, A.; Hüpkes, J.; Merdzhanova, T. Thin-Film Silicon Solar Cells on Dry Etched Textured Glass. *Energy Procedia* **2014**, *44*, 151−159.
(23) Jäger, K.; Linssen, D. N. P.; Isabella, O.; Zeman, M. Optimized Nano-Textured Interfaces for Thin-Film Silicon Solar Cells: Identifying the Limit of Randomly Textured Interfaces. In *Proceedings of SPIE 9140, Photonics for Solar Energy Sysems V*; Brussels, Belgium, April 14, 2014 ; SPIE: Bellingham, WA, 2014; Vol. *9140*, pp 91400M-1−91400M-9.
(24) Faÿ, S.; Steinhauser, J.; Nicolay, S.; Ballif, C. Polycrystalline ZnO:B Grown by LPCVD as TCO for Thin Film Silicon Solar Cells. *Thin Solid Films* **2010**, *518*, 2961−2966.
(25) Sever, M.; Lipovšek, B.; Krč, J.; Čampa, A.; Sánchez Plaza, G.; Haug, F.-J.; Duchamp, M.; Soppe, W.; Topič, M. Combined Model of Non-Conformal Layer Growth for Accurate Optical Simulation of Thin-Film Silicon Solar Cells. *Sol. Energy Mater. Sol. Cells* **2013**, *119*, 59−66.
(26) Hänni, S.; Alexander, D. T. L.; Ding, L.; Bugnon, G.; Boccard, M.; Battaglia, C.; Cuony, P.; Escarré, J.; Parascandolo, G.; Nicolay, S.; Cantoni, M.; Despeisse, M.; Meillaud, F.; Ballif, C. On the Interplay between Microstructure and Interfaces in High-Efficiency Microcrystalline Silicon Solar Cells. *IEEE J. Photovoltaics* **2013**, *3*, 11−16.
(27) Sever, M.; Krč, J.; Topič, M. Prediction of Defective Regions in Optimisation of Surface Textures in Thin-Film Silicon Solar Cells Using Combined Model of Layer Growth. *Thin Solid Films* **2014**, *573*, 176−184.
(28) Duchamp, M.; Lachmann, M.; Boothroyd, C. B.; Kovács, A.; Haug, F.-J.; Ballif, C.; Dunin-Borkowski, R. E. Compositional Study of Defects in Microcrystalline Silicon Solar Cells Using Spectral Decomposition in the Scanning Transmission Electron Microscope. *Appl. Phys. Lett.* **2013**, *102*, 133902−1−133902−3.
(29) Kaiser, I.; Nickel, N. H.; Fuhs, W.; Pilz, W. Hydrogen-Mediated Structural Changes of Amorphous and Microcrystalline Silicon. *Phys. Rev. B* **1998**, *58*, R1718−R1721.
(30) Droz, C.; Vallat-Sauvain, E.; Bailat, J.; Feitknecht, L.; Meier, J.; Shah, A. Relationship between Raman Crystallinity and Open-Circuit Voltage in Microcrystalline Silicon Solar Cells. *Sol. Energy Mater. Sol. Cells* **2004**, *81*, 61−71.
(31) Merdzhanova, T.; Carius, R.; Klein, S.; Finger, F.; Dimova-Malinovska, D. Defect States in Microcrystalline Silicon Probed by Photoluminescence Spectroscopy. *Thin Solid Films* **2006**, *511−512*, 394−398.
(32) Collins, R. W.; Ferlauto, A. S.; Ferreira, G. M.; Chen, C.; Koh, J.; Koval, R. J.; Lee, Y.; Pearce, J. M.; Wronski, C. R. Evolution of Microstructure and Phase in Amorphous, Protocrystalline, and Microcrystalline Silicon Studied by Real Time Spectroscopic Ellipsometry. *Sol. Energy Mater. Sol. Cells* **2003**, *78*, 143−180.
(33) Faÿ, S.; Kroll, U.; Bucher, C.; Vallat-Sauvain, E.; Shah, A. Low Pressure Chemical Vapour Deposition of ZnO Layers for Thin-Film Solar Cells: Temperature-Induced Morphological Changes. *Sol. Energy Mater. Sol. Cells* **2005**, *86*, 385−397.
(34) Beyer, W.; Hüpkes, J.; Stiebig, H. Transparent Conducting Oxide Films for Thin Film Silicon Photovoltaics. *Thin Solid Films* **2007**, *516*, 147−154.
(35) Luque, A.; Hegedus, S. *Handbook of Photovoltaic Science and Engineering*, 2nd ed.; John Wiley & Sons: Chichester, U.K., 2003.
(36) Hänni, S. Microcrystalline Silicon for High-Efficiency Thin-Film Photovoltaic Devices. Ph.D. Thesis, École Polytechnique Fédérale de Lausanne, Lausanne, Switzerland, 2014.
(37) Krč, J.; Zeman, M.; Kluth, O.; Smole, F.; Topič, M. Effect of Surface Roughness of ZnO:Al Films on Light Scattering in Hydrogenated Amorphous Silicon Solar Cells. *Thin Solid Films* **2003**, *426*, 296−304.
(38) Couty, P.; Duchamp, M.; Söderström, K.; Kovács, B. A.; Dunin-Borkowski, R. E.; Sansonnens, L.; Ziegler, Y.Transmission Electron Microscopy of Amorphous Tandem Thin-Film Silicon Modules Produced by a Roll-to-Roll Process on Plastic Foil. In *Proceedings of the 26th European Photovoltaic Solar Energy Conference*; Hamburg, Germany ; WIP: Munich, Germany, 2011; pp 2395−2398.
(39) Li, H. B. T.; Franken, R. H.; Rath, J. K.; Schropp, R. E. I. Structural Defects Caused by a Rough Substrate and Their Influence on the Performance of Hydrogenated Nano-Crystalline Silicon N−I−P Solar Cells. *Sol. Energy Mater. Sol. Cells* **2009**, *93*, 338−349.
(40) Hänni, S.; Bugnon, G.; Parascandolo, G.; Boccard, M.; Escarré, J.; Despeisse, M.; Meillaud, F.; Ballif, C. High-Efficiency Microcrystalline Silicon Single-Junction Solar Cells. *Prog. Photovoltaics* **2013**, *21*, 821−826.
(41) Sai, H.; Koida, T.; Matsui, T.; Yoshida, I.; Saito, K.; Kondo, M. Microcrystalline Silicon Solar Cells with 10.5% Efficiency Realized by Improved Photon Absorption via Periodic Textures and Highly Transparent Conductive Oxide. *Appl. Phys. Express* **2013**, *6*, 104101−1−104101−4.
(42) Sai, H.; Saito, K.; Hozuki, N.; Kondo, M. Relationship between the Cell Thickness and the Optimum Period of Textured Back Reflectors in Thin-Film Microcrystalline Silicon Solar Cells. *Appl. Phys. Lett.* **2013**, *102*, 053509−1−053509−5.